Transaction of the Korean Society of Mechanical Engineers, Vol. 10, No. 2, pp. 265~270, 1986.

<Original>

Effects of Conductivity and Thickness on Natural Convection Heat Transfer from a Horizontal Circular Tube†

Han-Shik Chung*, Byung-Hee Kang* and Sun-Sok Kwon**

(Received November 9, 1985)

水平 圓筒管의 熱傳導率과 두께가 自然對流 熱傳達에 미치는 影響

鄭 漢 植·姜 秉 熙·權 純 錫

Key Words : Natural Convection(自然對流), Wall Conductivity(管熱傳導率), Wall Thickness (管두께), Radial Velocity(半徑方向速度), Angular Velocity(圓周方向速度)

抄 錄

$Ra=10^6$, $Pr=5$에서 管熱傳導率과 두께가 變化할 때의 單一水平管에서의 自然對流 熱傳達에 관하여 有限差分法을 利用하여 解析的으로 硏究하였다. $\delta_w/d_0=0.1$에서 管熱傳導率이 높을수록 높은 溫度와 높은 局所 누셀트 數를 나타내며, $\theta=20°$에서의 圓周方向速度는 $(r-r_0)\fallingdotseq 0.08$에서 最大가 되며 半徑方向速度는 $(r-r_0)\fallingdotseq 0.14$에서 最大가 된다. 管外壁溫度는 管 두께가 증가함에 따라 거의 유사하게 감소하였다. $K_w/K_f=75$에서 角度變位가 증가함에 따라 局所 누셀트數는 현저히 증가하나 管 두께가 증가함에 따라서는 감소한다.

$\delta_w/d_0=0.1$에서 平均 누셀트數와 平均 溫度는 無次元 熱傳導率이 증가함에 따라 $K_w/K_f\leq 15$에서는 현저히 증가하고, $K_w/K_f>15$에서는 平均 누셀트 數는 서서히 증가하고 平均 溫度는 거의 같은 값을 가지며 指數函數로 表示할 수 있었다. $K_w/K_f=75, 50$에서 平均 누셀트數와 溫度는 無次元 管 두께가 증가함에 따라 거의 直線的으로 감소되며 線型 函數로 나타낼 수 있었다.

Nomenclature

Bi : Biot number, $h_i d_i/K_w$
d : Tube diameter
Ec : Eckert number, $\alpha^2 d_0^2/C_p\Delta T$
g : Gravitational acceleration
h : Convection heat transfer coefficient
K : Conductivity
Nu : Nusselt number, hd/K_f
Pr : Prandtl number, ν/α
R : Radial coordinate
Ra : Rayleigh number, $g\beta d_0^3\Delta T/\nu\alpha$
r : Dimensionless radial coordinate, R/d_0
U : Radial velocity
u : Dimensionless radial velocity, Ud_0/α
V : Angular velocity
v : Dimensionless angular velocity, Vd_0/α
W : Vorticity
w : Dimensionless vorticity, Wd_0/α
α : Thermal diffusivity
β : Thermal coefficient of volumetric expansion
ΔT : Temperature difference, T_b-T_e

† Presented at the 1985 KSME Autumn Conference
* Member, Graduate School, Dong-A University
** Member, Department of Mechanical Engineering Dong-A University

δ_w : Tube wall thickness
θ : Angular coordinate
μ : Absolute viscosity
ν : Kinematic viscosity, μ/ρ
ρ : Density
ϕ : Dimensionless temperature, $(T-T_e)/\Delta T$
Ψ : Stream function
ψ : Dimensionless stream function, Ψ/α

Subscripts

b : Internal bulk fluid
e : External fluid
f : Fluid
i : Radial grid number, tube inside surface
j : Angular grid number
o : Tube outside surface
w : Tube wall

Superscript

$-$: Average value

1. Introduction

Natural convection is observed as a result of the motion of the fluid due to density changes arising from the heating process. Natural convection heat transfer has been considered to be an effective method, because fluid need not to be flowed compulsorily. Many theoretical and experimental studies have been performed on natural convection from vertical plates, fins and isothermal cylinders. Alexander[1] studied experimentally velocity and temperature distributions about a horizontal cylinder in natural convection heat transfer. In experimental heat transfer studied by Harahap and McManus[2] & Jones and Smith[3], total heat transfer rates in air were determined from isothermal fin array attached to a base plate.

The heat transfer near the fin base was found to be very low whereas the largest local heat fluxes occurred near the upstream fin tip and leading edge of the base plate. Kuehn and Goldstein[4] solved Navier-Stokes equation and energy equation for natural convection heat transfer at a horizontal cylinder by numerical method, and then compared numerical solutions with the results of experiment. Kuehn and Balvanz[5] obtained numerical solution for conjugate heat transfer by natural convection from a horizontal heat exchanger tube. Kwon, Kuehn and Tolpadi[6] reported the results of heat transfer from a short vertical longitudinal fin below a heated horizontal cylinder for considering the influence of fin length on local and total heat transfer from a finned cylinder in water. Kwon and Kuehn[7] obtained numerical solutions for natural convection from a infinitely long conductive fin mounted vertically on an isothermal cylinder. The local heat transfer from the fin agreed with the similarity solution[8], except near the cylinder where boundary layers overlapped. The present study was undertaken to determine the enhancement of heat transfer by natural convection from heat exchanger tube immersed in liquids such as those used in process heating or in thermal storage tanks. In this study, on the basis of the Rayleigh number 10^6, Prandtl number 5, dimensionless wall conductivities 1~75 and dimensionless wall thickness 0.06~0.15, the characteristics of natural convection heat transfer has been calculated by finite difference method.

2. Numerical Solution

The geometry investigated are shown schematically in Fig. 1. The internal flow is fully forced convection of a warm liquid with bulk temperature T_b, uniform convective coefficient h_i and thermal conductivity K_f. The tube is assumed to have smooth interior and exterior surface and it has a uniform thermal conductivity K_w and uniform wall thickness δ_w. The following assumption can be made to simplify general Navier-Stokes and energy equation. Fluid

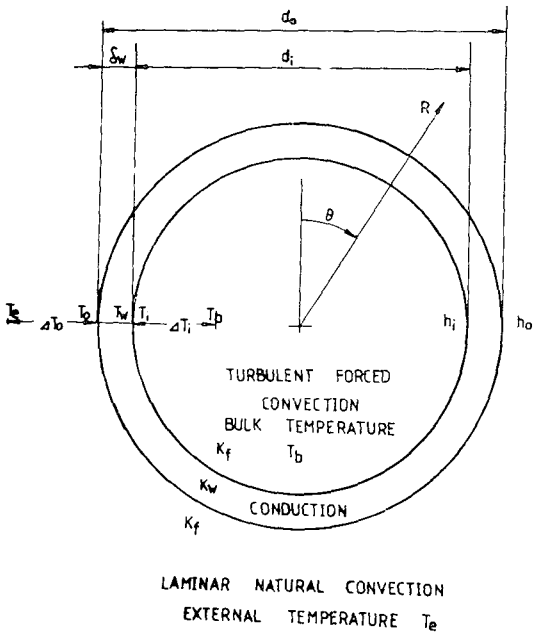

Fig. 1 Schematic diagram of the geometry investigated

is a state of incompressible laiminar flow and radiation heat transfer and viscous dissipation is considered to be negligible. The dimensionless equations for steady, laminar and natural-convection flow can be written in cylindrical polar coordinates using the Boussinesq approximation as follows[5]

$$\nabla^2\phi_w=0 \tag{1}$$

$$\nabla^2\phi=-w \tag{2}$$

$$\nabla^2 w=-\frac{1}{Pr}\left(u\frac{\partial w}{\partial r}+\frac{v}{r}\frac{\partial w}{\partial\theta}\right)-Ra\left(\sin\theta\frac{\partial\phi}{\partial r}+\frac{\cos\theta}{r}\frac{\partial\phi}{\partial\theta}\right) \tag{3}$$

$$\nabla^2\phi=\left(u\frac{\partial\phi}{\partial r}+\frac{v}{r}\frac{\partial\phi}{\partial\theta}\right)+EcPr\left[2\left\{\left(\frac{\partial u}{\partial r}\right)^2+\frac{1}{r^2}\left(\frac{\partial v}{\partial\theta}+u\right)^2\right\}+\left(\frac{1}{r}\frac{\partial u}{\partial\theta}+\frac{\partial v}{\partial r}-\frac{v}{r}\right)^2\right] \tag{4}$$

with

$$\nabla^2=\frac{\partial^2}{\partial r^2}+\frac{1}{r}\frac{\partial}{\partial r}+\frac{1}{r^2}\frac{\partial^2}{\partial\theta^2},$$

$$u=\frac{1}{r}\frac{\partial\psi}{\partial\theta},\quad v=-\frac{\partial\psi}{\partial r}$$

Equation (1) governs the temperature distribution within the tube wall and equation (2), (3) and (4) are applied to the external fluid. The viscous dissipation term in equation (4) is not used in this calculation, but is included for completeness. The flow is considered to be symmetric about the vertical plane passing through the center of the tube, so that the flow on one side needs to be solved. The dimensionless boundary conditions are shown in detail in Fig. 2.

$$\frac{K_w}{K_f}\frac{\partial\phi_w}{\partial r}=\frac{\partial\phi}{\partial r},\quad \phi_{wo}=\phi_o$$

$$u=v=\phi=0,\quad w=-\frac{\partial^2\psi}{\partial r^2} \tag{5}$$

on the tube outside surface ($r=r_0=0.5$)

$$\frac{h_i d_i}{k_w}\cdot\frac{d_o}{d_i}(1.0-\phi_w)=Bi_i\frac{d_o}{d_i}(1.0-\phi_w)=-\frac{\partial\phi_w}{\partial r} \tag{6}$$

on the tube inside surface($r=r_i=0.5-\delta_w/d_o$), and

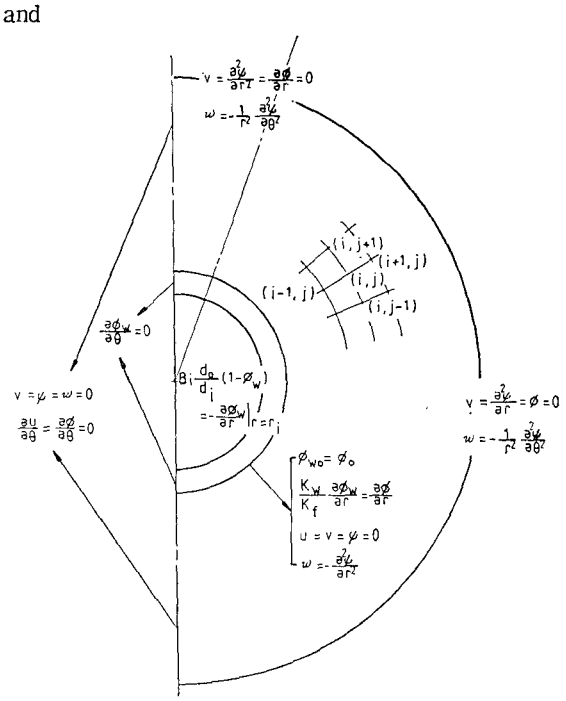

Fig. 2 Boundary conditions

$$v=\phi=w=\frac{\partial u}{\partial\theta}=\frac{\partial\phi}{\partial\theta}=\frac{\partial\phi_w}{\partial\theta}=0 \qquad (7)$$

on the symmetry lines.

The outer boundary must be treated as two parts; one with fluid coming into the solution domain, the other with fluid leaving, and the fluid is assumed to approach the tube radially at the ambient fluid temperature. The inflow boundary conditions for $20°\leq\theta\leq180°$ are

$$v=\frac{\partial^2\psi}{\partial r^2}=\phi=0 \qquad w=-\frac{1}{r^2}\frac{\partial^2\psi}{\partial\theta^2} \qquad (8)$$

and the outflow boundary conditions for $0°\leq\theta<20°$ are

$$v=\frac{\partial^2\psi}{\partial r^2}=\frac{\partial\phi}{\partial r}=0, \quad w=-\frac{1}{r^2}\frac{\partial^2\psi}{\partial\theta^2} \qquad (9)$$

An explicit successive over relaxation finite difference procedure is used to obtain solutions numerically. A hybrid differencing technique[9] is used for vorticity and temperature in the external fluid in which the coefficients are based on central differencing in regions of low velocity and small grid spacing, and upwind differencing in regions of high velocity and large grid spacing to prevent negative coefficients to lead to divergence. The majority of the solutions were obtained by using a 29×35 grid. The angular grid spacing was 0.625° at the top and bottom of tube in order to resolve the sharp angular gradients. The spacing doubles in steps to 10° for the majority of the 35 angular grid lines around the tube. The radial grid spacing was increased by $2\times\Delta ri$, $4\times\Delta ri$.... The radial grid within the tube is uniform with a maximum of 20 grid lines. The detail grid system is shown in Fig. 3. The solution was considered to be converged when both the stream function and temperature met the following criterion.

$$\left|\frac{B^m-B^{m-1}}{B^m}\right|<10^{-3} \qquad (10)$$

where, B is either stream function ϕ or temperature ϕ, and m is current iteration number. Calculations were performed on a IBM 370 computer with Fortran program. Solutions are typically obtained after 300~600 iterations with a CPU time of approximately 20 minutes.

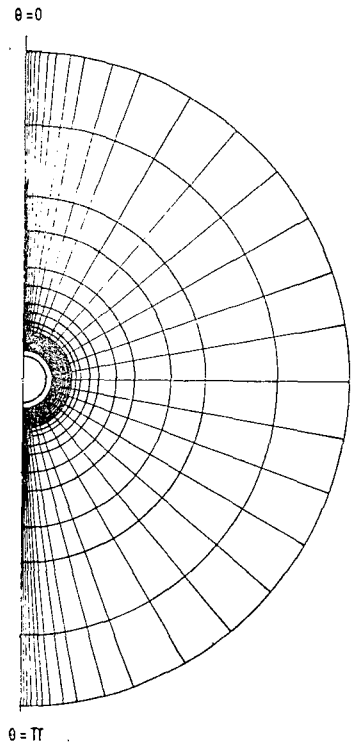

Fig. 3 Grid system

3. Results and Discussion

Numerical solutions have been obtained for a circular tube in which the Rayleigh number and Prandtl number were fixed at $Ra=10^6$ and $Pr=5$, but the wall conductivity and wall thickness of tube were varied. A plot of the dimensionless stream lines and isotherms is given in Fig. 4. The external surface temperature distributions as a function of angle and wall conductivity are shown in Fig. 5, at $\delta_w/d_0=0.1$. The temperature at the top portion is shown high by the effect of heated fluid, and the temperature is decreased by the activity of heat transfer to the bottom portion. Higher wall conductivity creates higher temperature, lower

wall conductivity creates lower temperature. The local Nusselt number distributions corresponding to the results shown in Fig. 5 are given in Fig. 6. The highest wall conductivity ratio, $K_w/K_f=75$, provides the largest variation in external heat transfer but little variation in wall temperature.

Low values of wall conductivity provide fairly uniform local Nusselt number but considerable changes in wall temperature. The fluid radial velocity distributions over the tube at $(r-r_0)=$

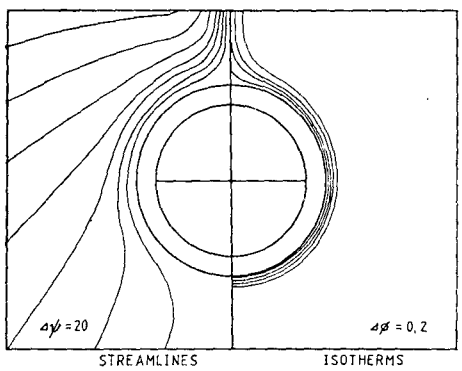

Fig. 4 Dimensionless streamlines and isotherms for conducting tube, $Ra=10^6$, $Pr=5$, $\delta_w/d_0=0.10$, $K_w/K_f=75$, $Nu_i=122.5$

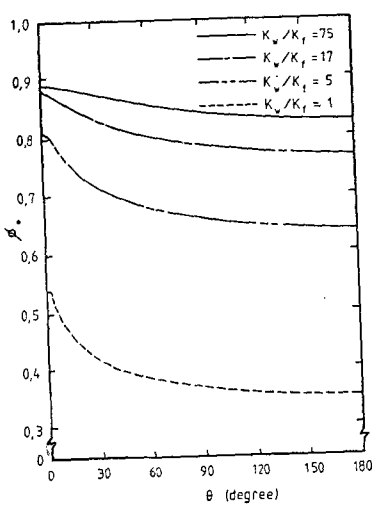

Fig. 5 Temperature distributions along external surface of conducting tube at $Ra=10^6$, $Pr=5$, $\delta_w/d_0=0.1$, $Nu_i=122.5$

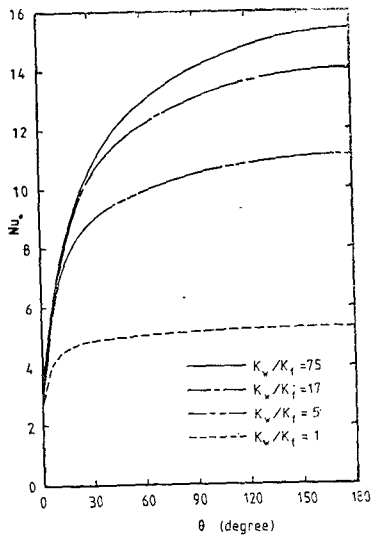

Fig. 6 Local Nusselt number distributions along external surface of conducting tube at $Ra=10^6$, $Pr=5$, $\delta_w/d_0=0.1$, $Nu_i=122.5$

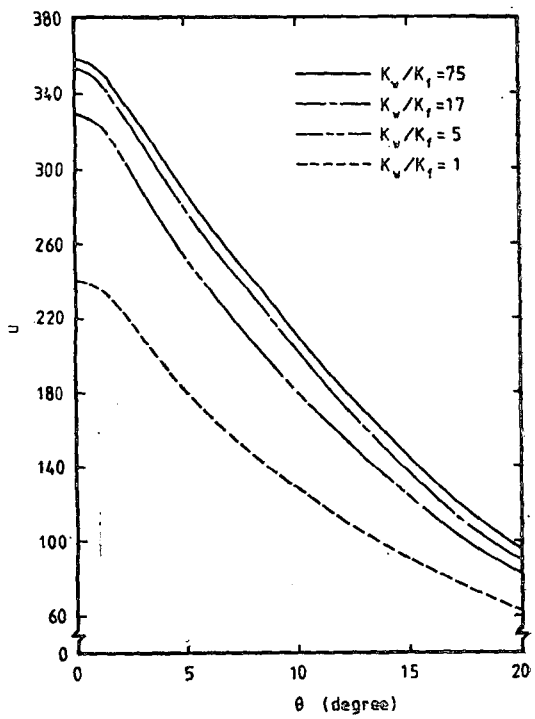

Fig. 7 Fluid radial velocity distributions at $(r-r_0)=0.1$, $Ra=10^6$, $Pr=5$, $\delta_w/d_0=0.1$, $Nu_i=122.5$

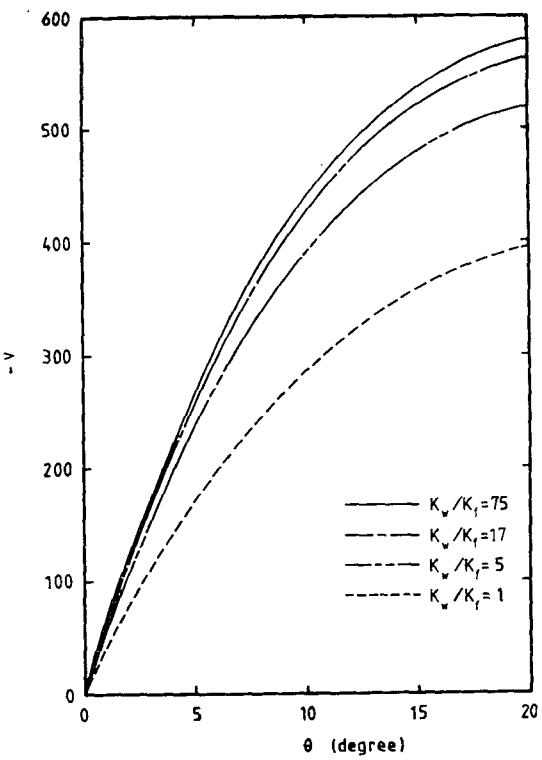

Fig. 8 Fluid angular velocity distribution at $(r-r_0)=0.1$, $Ra=10^6$, $Pr=5$, $\delta_w/d_0=0.10$, $Nu_i=122.5$

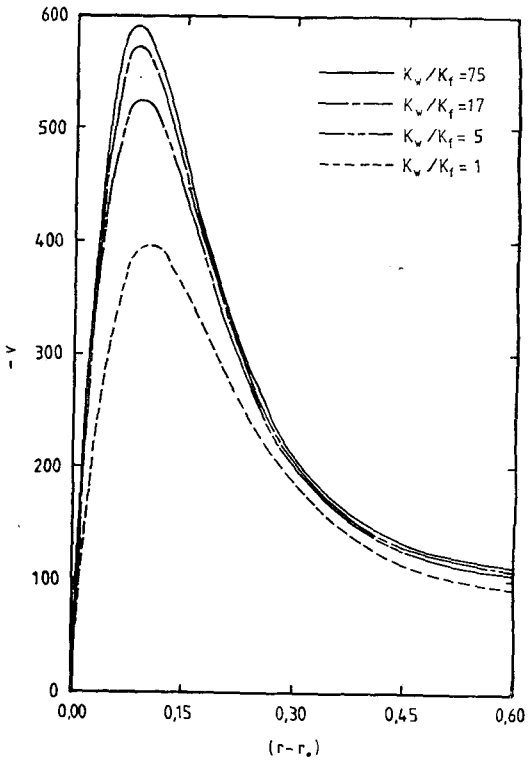

Fig. 9 Fluid angular velocity distributions at $\theta=20°$, $Ra=10^6$, $Pr=5$, $\delta_w/d_0=0.1$, $Nu_i=122.5$

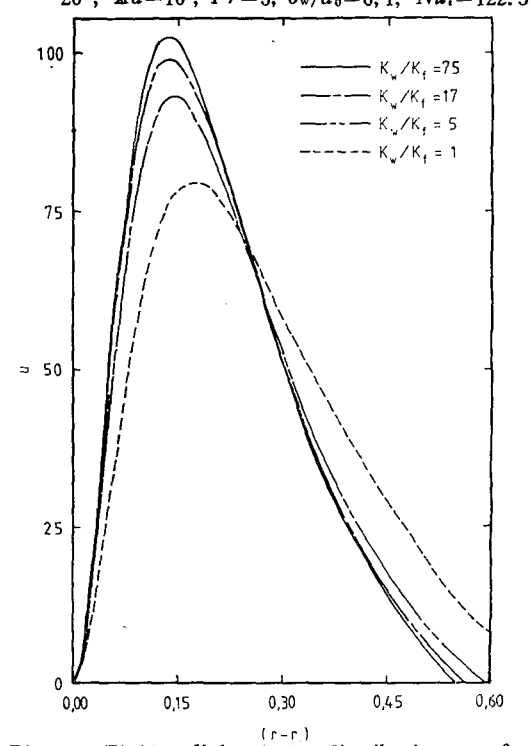

Fig. 10 Fluid radial velocity distributions at $\theta=20°$, $Ra=10^6$, $Pr=5$, $\delta_w/d_0=0.1$, $Nu_i=122.5$

0.1 are shown in Fig. 7. The radial velocity increases at the top portion, but the velocity decreases as the angle is increased. This result comes from the enhancing effect of the buoyance produced by heated tube. The angular velocity, however, is zero at $\theta=0°$ and then increases as the angle is increased, in Fig. 8. Also, higher wall conductivity creates higher velocity because plume is more active by the heated fluid around the tube. Fig. 9 gives the fluid angular velocity distributions at $\theta=20°$, $\delta_w/d_0=0.1$. The angular velocity near the tube increases remarkably and reaches maximum value to $(r-r_0)\cong 0.08$, and then rapidly decreased at $0.08<(r-r_0)\leq 0.4$, and gradually decreased at $(r-r_0)>0.4$. Fluid angular velocity have little effect by thermal conductivity at $K_w/K_f>10$. Fig. 10 shows fluid radial vel-

ocity distributions at $\theta=20°$, $\delta_w/d_0=0.1$. By increasing wall conductivity, the radial velocity is apparently increased at $(r-r_0)\leq 0.14$ and then apparently decreased at $(r-r_0)>0.14$, the velocity, therefore, reaches maximum value at $(r-r_0)\cong 0.14$. Higher wall conductivity has been known to be represented in higher velocity at $(r-r_0)\leq 0.24$ and in lower velocity at $(r-r_0)>0.24$. The temperature distributions along external surface of conducting tube at $K_w/K_f=75, 50$ are represented in Fig. 11 and 12. By increasing the dimensionless wall thickness from 0.06 to 0.15, the temperature distribution is decreased about 5.6% and the temperature of the top portion is higher than that of the bottom portion by the influence of tube wall heat transfer. The temperature distributions for various wall thickness show similar curves. Local Nusselt number distributions along external surface as a function of angle and wall thickness are

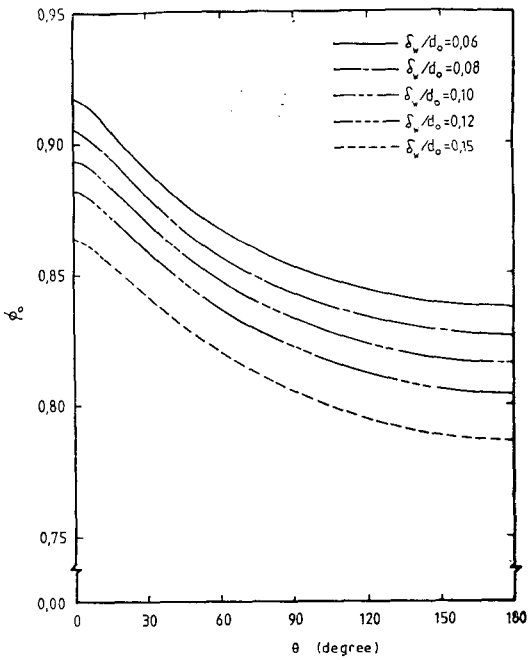

Fig. 12 Temperature distributions along external surface of conducting tube at $Ra=10^6$, $Pr=5$, $K_w/K_f=50$, $Nu_i=122.5$

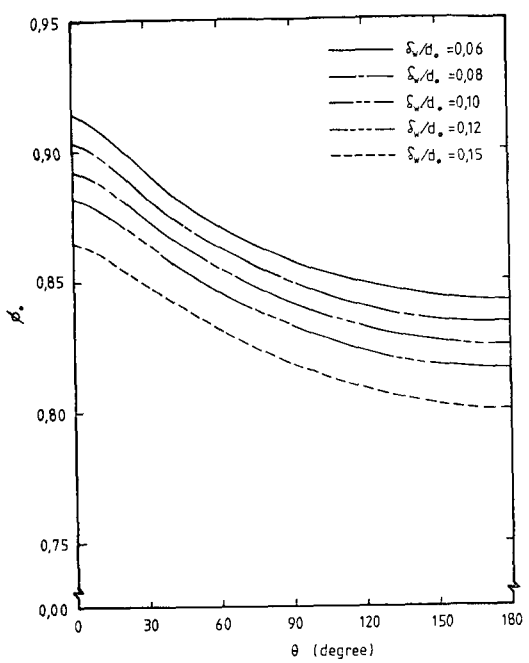

Fig. 11 Temperature distributions along external surface of conducting tube at $Ra=10^6$, $Pr=5$, $K_w/K_f=75$, $Nu_i=122.5$

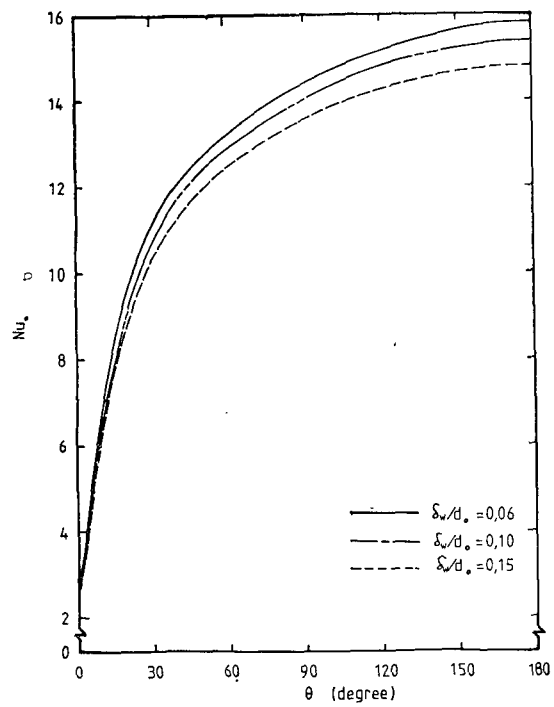

Fig. 13 Local Nusselt number distributions along external surface of conducting tube at $Ra=10^6$, $Pr=5$, $K_w/K_f=75$, $Nu_i=122.5$

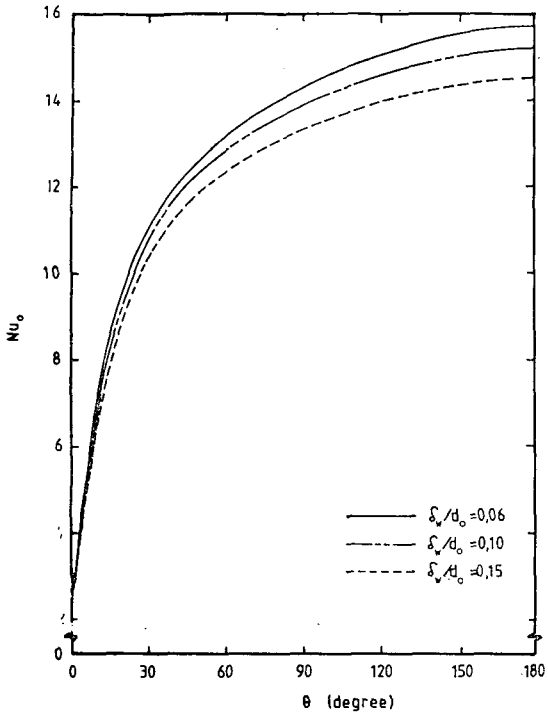

Fig. 14 Local Nusselt number distributions along external surface of conducting tube at $Ra=10^6$, $Pr=5$, $K_w/K_f=50$, $Nu_i=122.5$

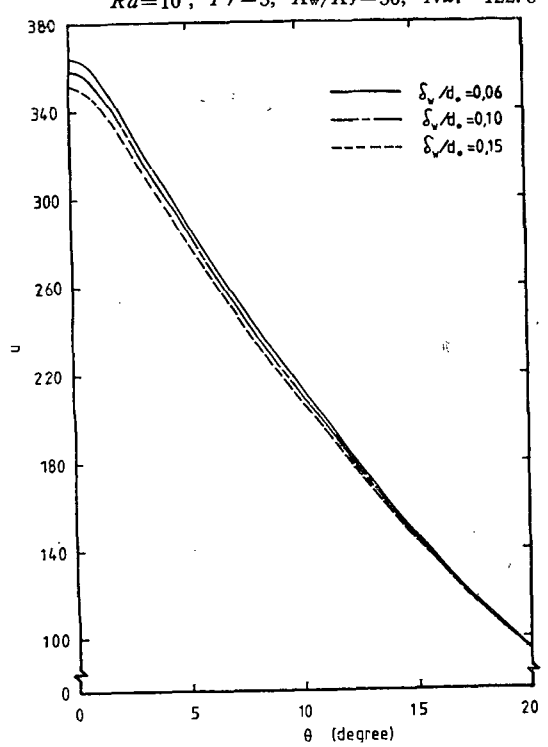

Fig. 15 Fluid radial velocity distributions at $(r-r_0)=0.1$, $Ra=10^6$, $Pr=5$, $K_w/K_f=75$, $Nu_i=122.5$

given in Fig. 13 and 14. Lower wall thickness creates higher local Nusselt number. Local Nusselt number increases apparently as the angle is approached at the bottom portion. Fig. 15 shows fluid radial velocity distributions near the top portion at $(r-r_0)=0.1$, $K_w/K_f=75$. As the angle is increased, radial velocity drops apparently. Fluid angular velocity distributions at $(r-r_0)=0.1$, $K_w/K_f=75$ are given Fig. 16. As the angle is increased, angular velocity is apparently increased. Mean Nusselt number and mean temperature distribution at $\delta_w/d_0=0.1$ are shown in Fig. 17. At $K_w/K_f\leq 15$, mean Nusselt number and temperature are apparently increased, and at $K_w/K_f>15$, mean Nusselt number is slightly increased but mean temperature shows same trend. As a result, the influence of wall conductivity has large at $K_w/K_f\leq 15$. From

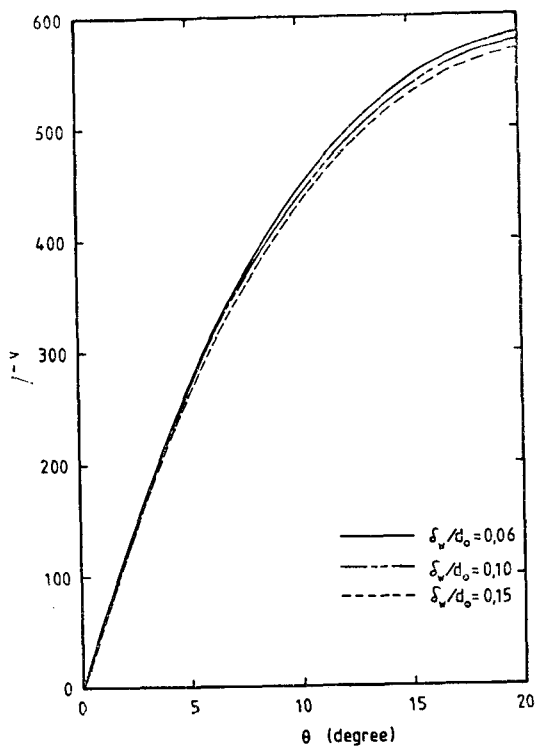

Fig. 16 Fluid angular velocity distributions at $(r-r_0)=0.1$, $Ra=10^6$, $Pr=5$, $K_w/K_f=75$, $Nu_i=122.5$

these results, mean Nusselt number and mean wall temperature can be represented by the following equations in exponential function for wall conductivities, $K_w/K_f=1\sim75$.

$$\bar{Nu}_0=13.09-9.603e^{-(K_w/K_f)}-4.921e^{-(K_w/K_f)}/10.25 \quad (11)$$

$$\bar{\phi}_0=0.85-0.580e^{-(K_w/K_f)}-0.275e^{-(K_w/K_f)}/10.25 \quad (12)$$

The comparisons between numerical results and equations (11), (12) are given in Table 1, and the errors between them show within 1.70%. The maximum error for mean Nusselt number is 1.70% at $K_w/K_f=10$ and for mean wall temperature is 1.49% at $K_w/K_f=10$. As the

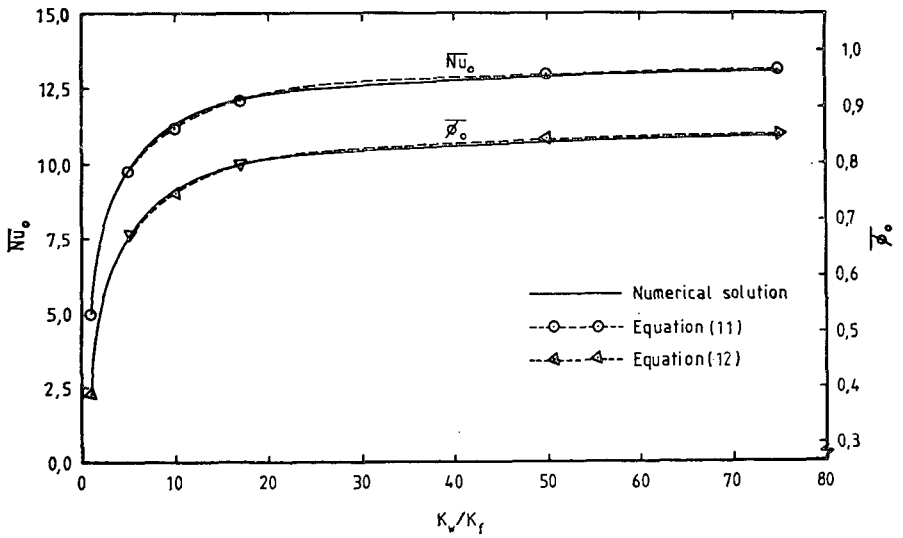

Fig. 17 Effect of wall conductivity on mean Nusselt number and wall temperature at $Ra=10^6$, $Pr=5$, $\delta_w/d_0=0.10$, $Nu_i=122.5$

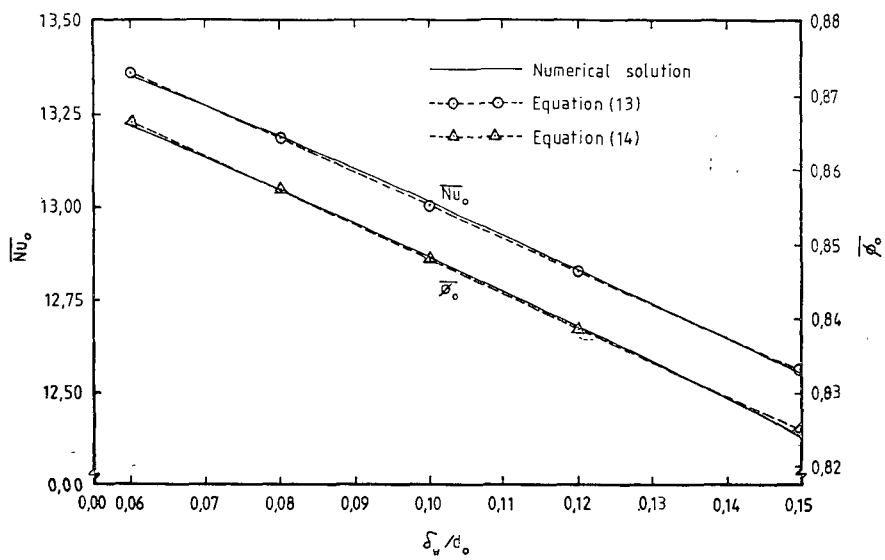

Fig. 18 Effect of wall thickness on mean Nusselt number and wall temperature at $Ra=10^6$, $Pr=5$, $K_w/K_f=75$, $Nu_i=122.5$

Table 1 *Comparison of mean Nusselt number and mean wall temperature for numerical solutions and equations (11), (12) for various wall conductivity at* $\delta_w/d_0=0.1$, $Ra=10^6$, $Pr=5$

K_w/K_f	$\overline{Nu}_0$			$\overline{\phi}_0$		
	Numerical	Equation(11)	Error(%)	Numerical	Equation(12)	Error(%)
1	5.05213	5.05368	0.03	0.38660	0.38665	0.01
5	9.95907	9.96394	0.04	0.67696	0.67704	0.01
10	11.38836	11.19453	1.70	0.75752	0.74618	1.49
17	12.10797	12.11296	0.04	0.79740	0.79757	0.02
50	12.87883	13.01254	1.03	0.84051	0.84790	0.87
75	13.02054	13.04673	0.20	0.84857	0.84790	0.07

Table 2 Comparison of mean Nusselt number and mean wall temperature for numerical solutions and equations (13), (14) for various wall thickness at $K_w/K_f=75$, $Ra=10^6$, $Pr=5$

δ_w/d_0	$\overline{Nu}_0$			$\overline{\phi}_0$		
	Numerical	Equation(13)	Error(%)	Numerical	Equation(14)	Error(%)
0.06	13.35479	13.36235	0.05	0.86597	0.86633	0.04
0.08	13.18459	13.18353	0.01	0.85722	0.85705	0.02
0.10	13.02054	13.00470	0.12	0.84857	0.84776	0.09
0.12	12.83871	12.82588	0.10	0.83919	0.83848	0.08
0.15	12.55247	12.55764	0.04	0.82418	0.82454	0.04

Table 3 Comparison of mean Nusselt number and mean wall temperature for numerical solutions and equations (15), (16) for various wall thickness at $K_w/K_f=50$, $Ra=10^6$, $Pr=5$

δ_w/d_0	$\overline{Nu}_0$			$\overline{\phi}_0$		
	Numerical	Equation(15)	Error(%)	Numerical	Equation(16)	Error(%)
0.06	13.26581	13.26644	0.01	0.86108	0.86166	0.06
0.08	13.07097	13.06265	0.06	0.85078	0.85071	0.01
0.10	12.87883	12.85886	0.15	0.84051	0.83976	0.08
0.12	12.67185	12.65507	0.13	0.82952	0.82881	0.08
0.15	12.34928	12.34938	0.01	0.81235	0.81238	0.01

wall thickness increases, mean Nusselt number and mean wall temperature at $K_w/K_f=75$ are decreased as shown in Fig. 18. From these results, mean Nusselt number and mean wall temperature can be induced by the following equations in linear function for wall thicknesses, $\delta_w/d_0=0.06\sim0.15$.

$$\overline{Nu}_0=13.90-8.94(\delta_w/d_0) \quad (13)$$

$$\overline{\phi}_0=0.894-0.464(\delta_w/d_0) \quad (14)$$

The comparisons between numerical results and equations (13), (14) are shown in Table 2, and the errors between them show within 0.12%. The maximum error is 0.12% at $\delta_w/d_0=0.1$ for mean Nusselt number and for mean wall temperature is 0.09% at $\delta_w/d_0=0.1$. The distributions of mean Nusselt number and mean wall temperature for wall thickness at $K_w/K=50$ are represented in Fig. 19. Mean Nusselt number and mean wall temperature are decreased linearly in the same phenomenon as shown in Fig. 18. The correlative relation from these can be given by the following equations.

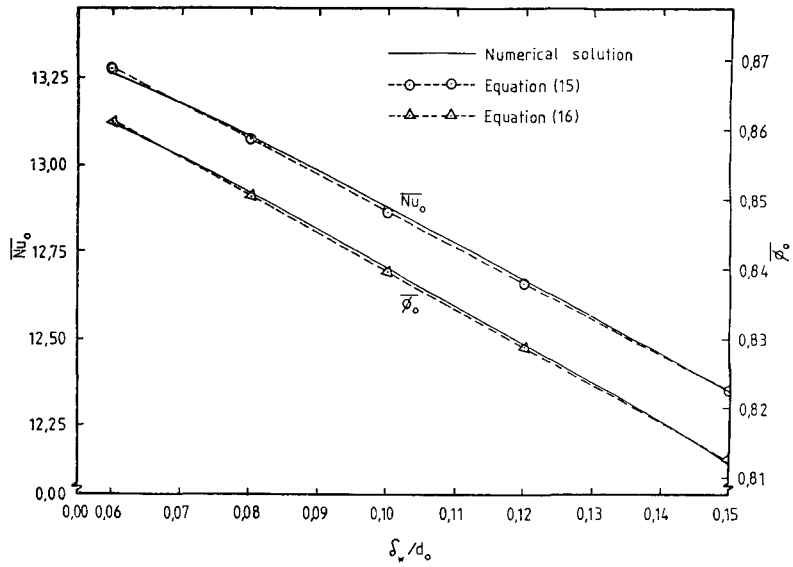

Fig. 19 Effect of wall thickness on mean Nusselt number and wall temperature at $Ra=10^6$, $Pr=5$, $K_w/K_f=50$, $Nu_i=122.5$

$$\overline{Nu}_0=13.88-10.19(\delta_w/d_0) \quad (15)$$

$$\bar{\phi}_0=0.895-0.548(\delta_w/d_0) \quad (16)$$

The errors between numerical results and equations (15), (16) show within 0.15% as shown in Table 3. The maximum error for mean Nusselt number is 0.15% at $\delta_w/d_0=0.1$ and for mean wall temperature is 0.08% at $\delta_w/d_0=0.1$.

4. Conclusions

The following conclusions, at $Ra=10^6$, $Pr=5$, can be made on the basis of the results presented above

(1) Higher wall conductivity creates higher wall temperature, and higher local Nusselt number at $\delta_w/d_0=0.1$.

(2) Angular velocity reaches maximum value at $(r-r_0)\cong 0.08$ and radial veloity reaches maximum value at $(r-r_0)\cong 0.14$ for external fluid at $\theta=20°$, $\delta_w/d_0=0.1$

(3) Temperature distributions along external surface of conducting tube are similarly decreased by increasing wall thickness.

(4) At $K_w/K_f=75$, local Nusselt number is apparently increased as the angle increases and the distributions decreased as wall thickness increased.

(5) Mean Nusselt number for $\delta_w/d_0=0.1$ is apparently increased at $K_w/K_f\leq 15$ and then slightly increases as wall conductivity increases and mean temperature shows a similar tendency, and for $K_w/K_f=75$, these values are decreased as wall thickness increases.

(6) Mean Nusselt numer and mean wall temperature can be represented by equations (11), (12) in exponential function for wall conductivity and by equations (13), (14), (15) and (16) in linear function for wall thickness.

References

(1) S. Alexander, "Velocity and Temperature Distributions about a Horizontal Cylinder in Free Convection Heat Transfer", AIChE Journal, Vol. 7, pp. 325~353, 1961

(2) F. Harahap and H.N. McManus, "Natural Con-

vection of Heat Transfer from Horizontal Rectangular Fin Arrays", J. Heat Transfer, Vol. 89, pp. 32~38, 1967

(3) C.D. Jones and L.T. Smith, "Optimum Arrangement of Rectangular Fins on Horizontal Surfaces for Free Convention Heat Transfer", J. Heat Transfer, Vol. 92, pp. 6~10, 1970

(4) T.H. Kuehn and R.J. Goldstein, "Numerical Solution to the Navier-Stokes Equations for Laminar Convection about a Horizontal Isothermal Circular Cylinder", Int. Journal of Heat and Mass Transfer, Vol. 23, pp. 971~979, 1980

(5) T.H. Kuehn and J.L. Balvanz, "Conjugate Heat Transfer by Natural Convection from a Horizontal Heat Exchanger Tube", Proc. 7th Heat Transfer Conference Vol. 2, pp. 317~322, 1982

(6) S.S. Kwon, T.H. Kuehn and A.K. Tolpadi, "Conjugate Natural Convection Heat Transfer from a Short Vertical Longitudinal Fin below a Heated Cylinder", ASME, 83-HT-100, pp. 1~8, 1983

(7) S.S. Kwon and T.H. Kuehn, "Conjugate Natural Convection Heat Transfer from a Horizontal Cylinder with a Long Vertical Longitudinal Fin". Numerical Heat Transfer, Vol. 6, pp. 85~102, 1982

(8) T.H. Kuehn, S.S. Kwon and A.K. Tolpadi, "Similarity Solution for Conjugate Natural Convection Heat Transfer from a Long Vertical Plate Fin, Int. J. Heat Mass Transfer, Vol. 26, No. 11, pp. 1718~1721, 1983

(9) S.V. Patankar, "Numerical Heat Transfer and Fluid Flow", pp. 40~111, McGraw-Hill Co., New York, 1980